Coupling of ToF-SIMS and Raman Spectroscopy for the Characterization of the Chemical Species Involved in the Soot Nucleation Process

Jessy Elias, Alessandro Faccinetto, Nicolas Nuns, Claire Pirim, Cristian Focsa, Xavier Mercier

Coupling of ToF-SIMS and Raman Spectroscopy for the Characterization of the Chemical Species Involved in the Soot Nucleation Process

J. Elias*[,1,2], A. Faccinetto[1], N. Nuns[3], C. Pirim[4], C. Focsa[4], X. Mercier[1]

[1]Univ. Lille, CNRS, UMR 8522 - PC2A - Physicochimie des Processus de Combustion et de l'Atmosphère, F-59000 Lille, France

[2]French Environment and Energy Management Agency, 20 avenue du Grésillé, F-49004 Angers, France

[3]Univ. Lille, M. E. Chevreul Institut, F-59000 Lille, France

[4]Univ. Lille, CNRS, UMR 8523 - PhLAM - Physique des Lasers, Atomes et Molécules, F-59000 Lille, France

Abstract

Time-of-flight secondary ion mass spectrometry (ToF-SIMS) and Raman spectroscopy are used to characterize samples extracted from a laboratory methane diffusion flame at different reaction times along the flame axis in order to gain information on the soot nucleation process. Experimental results from the comparison of these techniques allow the chemical characterization of the gas to soot particles phase transition and the quantification of the hydrogen content of the sampled matter. Before soot formation, no phase separation is observed on the samples, while after soot formation, a phase separation appears with two families of PAHs and a difference in the Raman signal.

Introduction

Despite the considerable number of experimental and theoretical studies performed during the last decades, a comprehensive view of the transition from molecular precursors to condensed phase particles (soot nucleation) in flames is still missing [1,2].

A common experimental approach to obtain information on soot nucleation relies on the online or ex-situ chemical analysis of the stable species adsorbed on the surface of soot particles sampled at various reaction times in flame environments. This approach proved to be highly successful and led in particular to the identification of polycyclic aromatic hydrocarbons (PAHs) and their derivatives as main soot precursors [3–5]. In this work, a set of samples was collected from the axis of a methane laminar diffusion flame and subsequently ex-situ characterized by secondary ion mass spectrometry (ToF-SIMS) and Raman spectroscopy. The results are combined with the aim of characterizing the nature of the molecular precursors involved in the formation of nascent soot particles.

The systematic use of ToF-SIMS for the analysis of the chemical composition of combustion byproducts is relatively recent [6–8]. While ToF-SIMS is highly sensitive to the surface composition of the samples, and in static mode can provide access to surface layers as thin as a few nm, the post-ionization dissociation and recombination processes are far from being fully understood, and the perspective of quantitative analyses remains challenging to date [9,10]. Therefore, statistical tools are often required to extract the large amount of chemical information contained in the mass spectra.

Raman spectroscopy has long been used to obtain quantitative information on carbon-based materials. For instance, empirical relationships to obtain the H/C ratio of carbon films from the slope of the fluorescence and the intensity of the G band have been proposed as early as two decades ago [11,12]. The intrinsically complex nature of combustion-generated materials and the existence of hydrocarbons adsorbed on the particle surface further adds to the spectral complexity of soot [13–16].

The main goal of this work is to provide additional information that can be used for the ex-situ characterization of soot particles extracted from a laboratory flame and deposited on metal substrates, that are for all practical purposes treated like the carbon films mentioned above. In particular, we aim to identify experimental parameters that can be used to pinpoint and if possible to characterize the transition from molecular precursors to condensed-phase particles. With respect to our previous investigation [7], in which we focused on the zone where nascent soot particles could first be detected by laser induced incandescence (LII), in this work we extend the investigated range to almost the entire flame height.

Experimental

In this work, measurements are performed on soot samples collected from a 120 mm height methane laminar diffusion flame, shown in Figure 1a, stabilized on a Santoro-type burner at atmospheric pressure. This burner consists of a central injector supplied with 0.546 L/min of methane and surrounded by a 86.6 L/min air flow. This flame is characterized by the stratified distribution of PAHs and soot particles through the centerline of the flame that can therefore be targeted independently during sampling [17]. Species are extracted from the flame using a dilutive quartz microprobe inserted radially and operated with nitrogen, in order to reduce the collision probability in the sampling line and limit their reactivity. The collected species are deposited on titanium wafers using a 1/8" diameter impactor. High velocity impaction of the species (~34 m/s) results in soot particles and other condensed-phase species aggregating at the center of the wafer and the condensable gas scattering all over the wafer surface as shown in Figure 1b. Therefore, ToF-

*Corresponding author: jessy.elias@univ-lille.fr

SIMS and Raman ex-situ measurements are performed, as detailed below, on two selected regions of interest (ROIs): the soot deposit (impaction ROIs) and the wafer surface surrounding it (halo ROIs). The mass spectra recorded on the impaction ROIs, where soot particles impacted (only detected for height above the burner HAB > 50 mm, as discussed below), contain the combined contributions of soot and condensable gas, while the mass spectra recorded on the halo ROIs only contain the contribution of condensable gas.

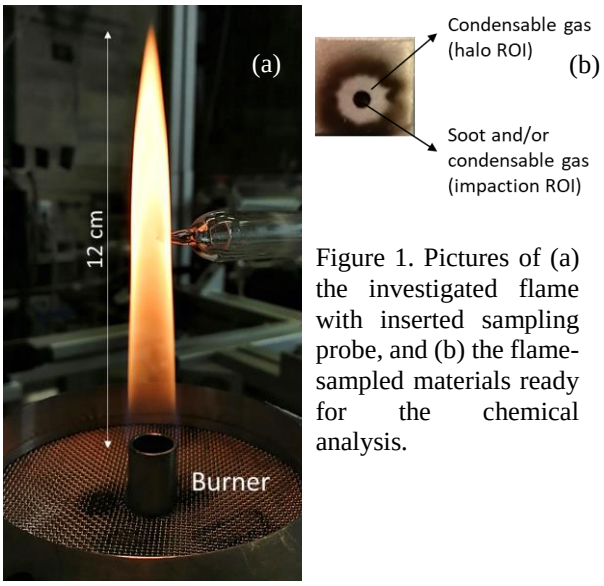

Figure 1. Pictures of (a) the investigated flame with inserted sampling probe, and (b) the flame-sampled materials ready for the chemical analysis.

ToF-SIMS is a sensitive surface analytical technique used to obtain information on the chemical composition of solid samples. In ToF-SIMS, a primary Bi_3^+ ion beam is used to sputter and ionize the compounds on the sample surface. The generated secondary ions, are accelerated and analyzed on a time-of-flight mass spectrometer with a mass resolution of $m/\Delta m = 10000$. This technique is sensitive to high mass organic compounds ($m/z > 200$) due to the use of Bi_3^+ ions having an energy of 25 keV with a very low current intensity of 0.3 pA in static mode. Mass spectra in positive polarity are recorded at 50 scans/acquisition on a 500 × 500 μm^2 surface with an image resolution of 128 × 128 pixels. Acquisitions are performed on three different zones on each ROI. The collected mass spectra are aligned, calibrated and normalized by the total useful ion count. ToF-SIMS mass spectra contain a significant amount of chemical information difficult to extract and require detailed data treatment. Peaks are identified using mass defect analysis [18], allowing the assignment of a molecular formula to the selected accurate masses. The vast majority of the attributed molecular formulae are consistent with PAHs or their derivatives. Then, an advanced statistical tool, the principal component analysis (PCA), is used to classify the data and explain the variance of the database. From a theoretical point of view, PCA is a series of linear transformations which project a set of correlated variables onto linearly uncorrelated variables denoted as principal components (PC). PCA is performed on the covariance matrix using the relative ion counts (normalized to the total useful ion count) of individual m/z as variables and ROIs of each sample as observations, in order to find statistically significant data correlations.

Raman spectroscopy analyses are carried out in order to obtain structural information on soot and characterize the gas/particle phase transition. The Raman microscope (InVia Reflex, Renishaw) is equipped with a $\lambda = 514.5$ nm diode-pumped solid-state laser. The laser power is reduced to 0.05% corresponding to a laser irradiance equal to 1627 W/cm^2 to avoid structural changes in the sample. The laser beam is focused on the samples with a 20x magnification objective. The Raman spectral intensity and wavelength are calibrated with a silicon wafer by utilizing the pure Si peak at 520 cm^{-1}. Instrument settings (grating 600 lines per mm and acquisition time 6 s with 80 accumulations) are chosen after a set of test measurements to provide the best signal-to-noise ratio for the analysis. About 30 Raman spectra per ROIs are recorded between 700 and 2500 cm^{-1} for each sample.

Results

The main results of the PCA performed on the mass spectra database after removing the background and fragment ions are shown in Figure 2. The matrix used for the PCA includes 529 peaks (variables) and 150 mass spectra (observations). Together, PC1 and PC2 explain the 74.25% of the total variance of the database. In the PC2 vs. PC1 score plot shown in Figure 1a, at least three different clusters of mass spectra can be identified:

- For HAB ≤ 35mm (yellow datapoints), no statistically significant difference is found between impaction and halo ROIs that appear all clustered together in the score plot and characterized by PC1 < 0.
- For 40 mm ≤ HAB ≤ 70 mm (orange-red datapoints), impaction and halo ROIs are split into two groups: impaction ROIs in PC1 < 0 while halo ROIs in PC1 > 0.
- For HAB ≥ 80 mm (black datapoints) impaction and halo ROIs are both in PC1 > 0, but they are split into two clusters in PC2.

The loading plots of PC1 and PC2, shown in Figure 2b and 2c respectively, give some insights on the variables affecting the PCs. PC1 < 0 is characterized by high loadings of high m/z hydrocarbons, while PC1 > 0 is characterized by high loadings of low m/z hydrocarbons. A sharp change of the PC1 sign is observed around 240 m/z (corresponding to C19 hydrocarbons). High scores in one PC means that the corresponding data are strongly affected by the variables characterizing that same PC. Thus, the mass spectra recorded in the impaction and halo ROIs at HAB ≤ 35 mm and in the impaction ROIs at 40 mm ≤ HAB ≤ 70 mm are characterized by the highest relative ion counts of high m/z hydrocarbons. On the other hand, the mass spectra recorded in the halo ROIs at 40 mm ≤ HAB ≤ 70 mm and in the impaction and halo

ROIs at HAB ≥ 80 mm are characterized by the highest relative ion counts of low *m/z* hydrocarbons. In other words, the transition from the left to the right of the score plot corresponds well to a progressive increase in the relative contribution to the mass spectra of low *m/z* hydrocarbons. Furthermore, the score plot strongly suggests that the phenomenon represented by the PC1 is HAB-dependent (the mass spectra are also sorted from the left to the right according to the sampling HAB). On the other hand, a clear clustering of the mass spectra on PC2 only occurs at 80, 90 and 100 mm HAB (impaction ROIs have PC2 > 0 and halo ROIs have PC2 < 0). The role of PC2 has not yet been identified.

As also shown in Figure 2, all Raman spectra at HAB ≤ 35 mm and the Raman spectra of the impaction ROIs at 40 mm ≤ HAB ≤ 70 mm feature high fluorescence background and intense bands at 1360 cm^{-1} and 1580 cm^{-1} that are characteristic of disordered graphite (D band) and graphitic lattices (G band) respectively [19]. These bands are absent in the halo ROIs at 40 mm ≤ HAB ≤ 70 mm.

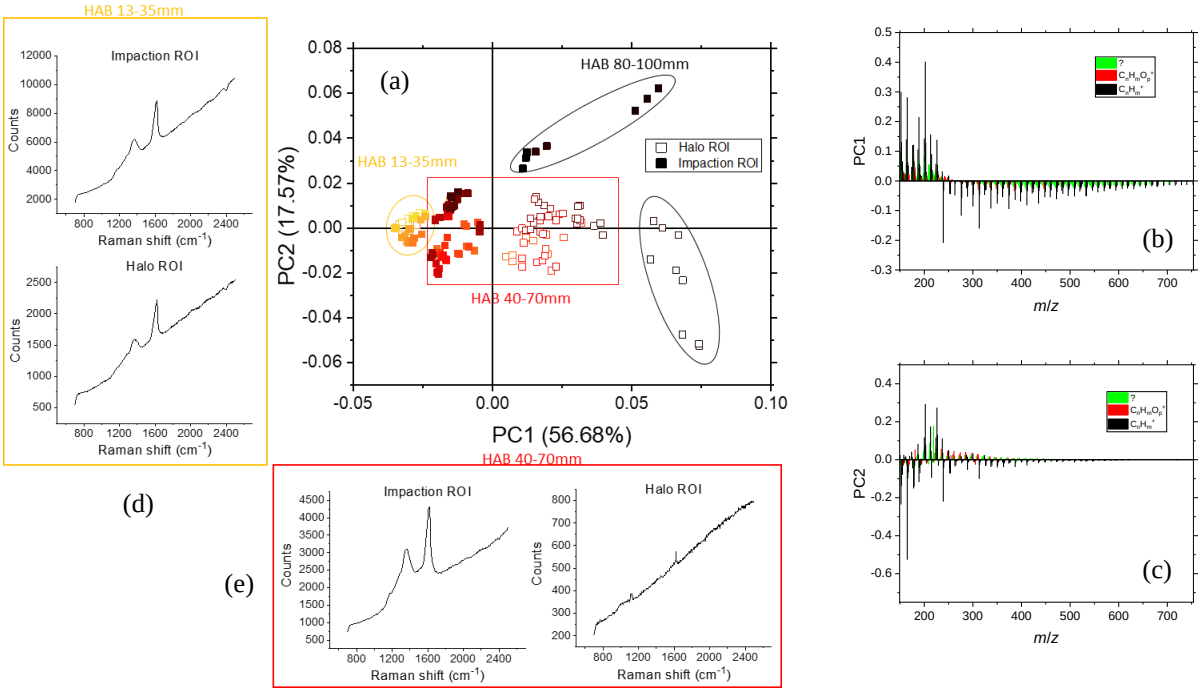

Figure 2. Results of the PCA on the full mass spectra database and comparison with Raman spectra without baseline correction. (a) PC2 vs. PC1 score plot. (b) PC1 loading plot. (c) PC2 loading plot. (d) Raman spectra on the impaction and halo ROIs before soot formation. (e) Raman spectra on the impaction and halo ROIs after soot formation.

Implications for the soot formation process

The comparison of ToF-SIMS and Raman measurements provides useful information on the global fraction of H atoms [H] as a function of the HAB in the flame that in turn can be used to gain insights into the soot nucleation process. $[H]_{ToF\text{-}SIMS}$ can be calculated by means of the peaks identified through mass defect analysis, where the normalized signal intensity of the mass spectra w_i is used to weight the individual contributions of the identified ions $N_{X,i}$ [7]:

$$[H]_{ToF-SIMS} = \frac{N_H}{N_H + N_C + N_O}$$

$$\text{with } N_X = \sum_i N_{X,i} w_i \,, X = H, C, O \text{ and } \sum_i w_i = 1$$

Figure 3a shows that hydrocarbons in halo ROIs (condensable gas only) continue to gain hydrogens all along the flame axis, while hydrocarbons in impaction ROIs (soot and/or condensable gas) undergo a loss in hydrogen between 45-55 mm HAB. This region is particularly significant as previous in-situ LII measurements performed on this flame show that nascent soot particles are detectable in the flame axis above 50 mm HAB [17]. Here, the change in chemical composition of the impaction and halo ROIs, potentially representing a change of phase, begins at 40 mm HAB, slightly below the previously detected LII signal. However, it must be noted that the experimental LII configuration used in our previous investigation [17] was not optimized for detecting the smallest particles, and therefore the existence of nascent soot particles between 50 and 55 mm HAB cannot be completely ruled out. This observation, even when considering the uncertainty due to the flame perturbation induced by the sampling microprobe (size of the sampled region < 1 mm, size of the perturbed flame region < 2.5 mm), shows that the change in the chemical composition of the samples occurs immediately before or at the same time as the detection of soot particles.

Experimental OH profiles measured by 1aser induced fluorescence (LIF) in this flame (not shown here) pinpoint the beginning of the soot oxidation region, identified by a sharp increase of the OH radical

concentration in the flame axis, at 70-75 mm HAB that corresponds to the second change of slope of $[H]_{ToF\text{-}SIMS}$ vs. HAB.

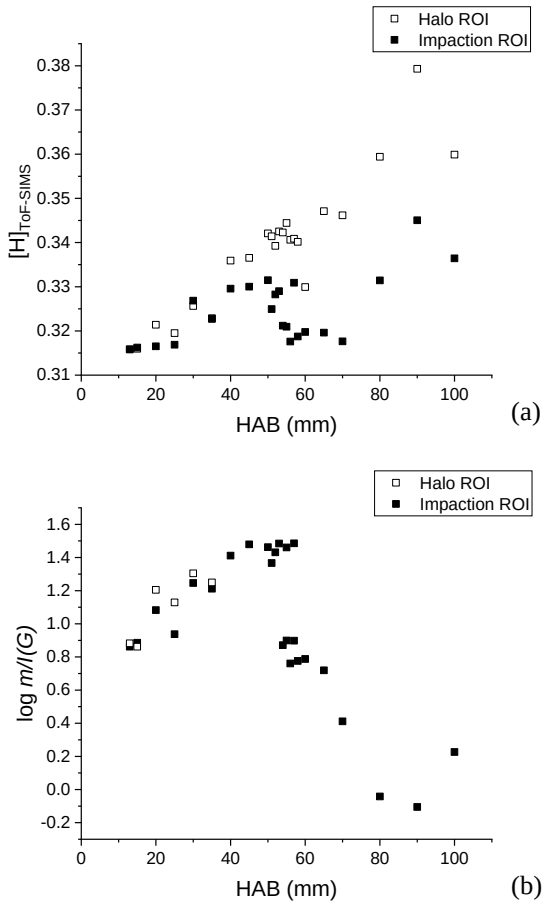

Figure 3. (a) $[H]_{ToF\text{-}SIMS}$ vs. HAB. (b) log m/*I*(G) vs. HAB.

$[H]_{Raman}$ has been shown to be proportional to log m/*I*(G), where m is the slope of the linear fit of the fluorescence background (in this work measured between 1000 and 2000 cm^{-1}), and *I*(G) is the intensity of the Raman G band [11,12]. As shown in Figure 3, the trends of $[H]_{ToF\text{-}SIMS}$ and log m/*I*(G) are remarkably consistent up to 65 mm HAB. In particular, although log log m/*I*(G) of the halo ROIs cannot be calculated due to the absence of the G band in the Raman spectra, log m/*I*(G) of the impaction ROIs, as shown in Figure 3b, exhibits a change of slope at the same HAB observed by ToF-SIMS. This local change of sign of the slope of [H] vs. HAB immediately before the detection of LII signal might be related to the soot formation process. Specifically, it could point to the formation of species bound by C-C covalent bonds possibly via a sequence of hydrogen abstraction reactions [20].

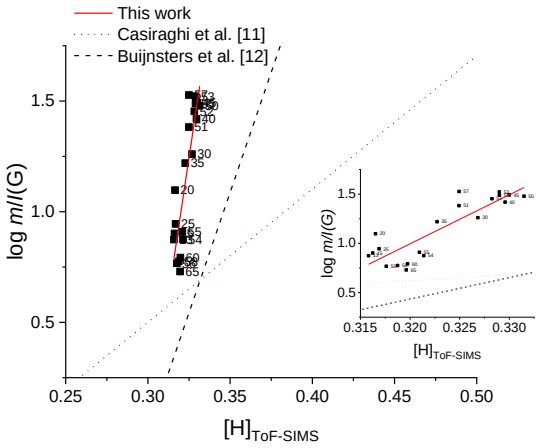

Figure 4. log m/*I*(G) vs. $[H]_{ToF\text{-}SIMS}$ and comparison with literature (impaction ROIs only).

Figure 4 compares the data obtained here with two empirical equations (blue dotted line and black dashed line) obtained from the analysis of amorphous hydrogenated carbon films prepared by chemical vapor deposition [11,12]. As shown in the figure, log m/*I*(G) of the impaction ROIs (red solid line) scales linearly with $[H]_{ToF\text{-}SIMS}$ up to 70 mm HAB ($R^2 = 0.7580$ that approximately corresponds to the beginning of the soot oxidation region mentioned above:

$$[H]_{ToF-SIMS} = -13.7 + 45.9 \log \frac{m}{I(G)}$$

The two empirical equations available in the literature differ significantly from each other. This work indicates a better agreement with the empirical equation proposed by Buijnsters et al. [12]. The deviation with respect to literature can be attributed to the different volume probed by the two techniques: ToF-SIMS in static mode affects a surface layer as thin as a few nm, while the penetration depth of the Vis laser beam used in this work for Raman spectroscopy is in the range of a few μm [21]. [

At HAB > 65 mm, a large deviation from linearity is observed, and therefore the HABs in the soot oxidation zone of the flame (70, 80, 90 and 100 mm) are not considered in the fitting procedure shown in Figure 4. This behavior is still unexplained and will require future investigations.

Conclusions and perspectives

In this work, samples extracted at different height above the burner (HAB) from a laboratory methane diffusion flame are analyzed by secondary ion mass spectrometry (ToF-SIMS) and Raman spectroscopy to gain information on the soot nucleation process.

For HAB ≤ 35 mm, well before nascent soot particles are detected by laser induced incandescence (LII), no phase separation is observed on the deposition substrates and all impaction sites have virtually the same chemical composition that includes the highest mass hydrocarbons detected all along the flame HAB. The Raman spectra are characterized by an intense fluorescence background and intense D and G Raman bands detected at 1360 cm^{-1} and 1580 cm^{-1}. Downstream from roughly 40 mm HAB, a

phase separation and the partition of organic molecules between the two phases are observed. The condensable gas is progressively depleted of high *m*/*z* PAHs (their signal in the mass spectra becomes less and less prominent, while the Raman D and G bands disappear), while high *m*/*z* PAHs persist when associated to the formation of soot particles. In particular, around 45 mm HAB both ToF-SIMS and Raman detect a change in the sign of the slope of [H] vs. HAB that might be related to the phase transition.

Future work include a full deconvolution of the Raman spectra into multiple bands (D4, D1', D1, D3, G and D2) to evaluate the significant spectral parameters (position of the bands, full width at half maximum and ratios of integrated intensity) following the flame central axis. The goal of this work is to expand the interpretation of the results obtained and the comparison with ToF-SIMS analysis in order to characterize the chemical species involved in the soot nucleation process in flame combustion.

Acknowledgments

This work was supported by the Agence Nationale de la Recherche through the LABEX CAPPA (ANR-11-LABX-0005), and the Ministry of Higher Education and Research, Hauts de France Regional Council, and European Regional Development Fund (ERDF) through the Contrat de Projets Etat Region (CPER CLIMIBIO). The authors also thank the Agency for ecological transition (ADEME) for the financial support of this project.

Bibliography

[1] A. D'Anna, Combustion-formed nanoparticles, Proc. Combust. Inst. 32 (2009) 593–613. https://doi.org/10.1016/j.proci.2008.09.005.

[2] H. Wang, Formation of nascent soot and other condensed-phase materials in flames, Proc. Combust. Inst. 33 (2011) 41–67. https://doi.org/10.1016/j.proci.2010.09.009.

[3] R.A. Dobbins, R.A. Fletcher, H.-C. Chang, The evolution of soot precursor particles in a diffusion flame, Combust. Flame. 115 (1998) 285–298. https://doi.org/10.1016/S0010-2180(98)00010-8.

[4] F. Schulz, M. Commodo, K. Kaiser, G. De Falco, P. Minutolo, G. Meyer, A. D`Anna, L. Gross, Insights into incipient soot formation by atomic force microscopy, Proc. Combust. Inst. 37 (2018) 885–892. https://doi.org/10.1016/j.proci.2018.06.100.

[5] B. Öktem, M.P. Tolocka, B. Zhao, H. Wang, M.V. Johnston, Chemical species associated with the early stage of soot growth in a laminar premixed ethylene–oxygen–argon flame, Combust. Flame. 142 (2005) 364–373. https://doi.org/10.1016/j.combustflame.2005.03.016.

[6] C. Irimiea, A. Faccinetto, X. Mercier, I.-K. Ortega, N. Nuns, E. Therssen, P. Desgroux, C. Focsa, Unveiling trends in soot nucleation and growth: When secondary ion mass spectrometry meets statistical analysis, Carbon. 144 (2019) 815–830. https://doi.org/10.1016/j.carbon.2018.12.015.

[7] A. Faccinetto, C. Irimiea, P. Minutolo, M. Commodo, A. D'Anna, N. Nuns, Y. Carpentier, C. Pirim, P. Desgroux, C. Focsa, X. Mercier, Evidence on the formation of dimers of polycyclic aromatic hydrocarbons in a laminar diffusion flame, Commun. Chem. 3 (2020) 112. https://doi.org/10.1038/s42004-020-00357-2.

[8] L.D. Ngo, D. Duca, Y. Carpentier, J.A. Noble, R. Ikhenazene, M. Vojkovic, C. Irimiea, I.K. Ortega, G. Lefevre, J. Yon, A. Faccinetto, E. Therssen, M. Ziskind, B. Chazallon, C. Pirim, C. Focsa, Chemical discrimination of the particulate and gas phases of miniCAST exhausts using a two-filter collection method, Atmos Meas Tech. 13 (2020) 951–967. https://doi.org/10.5194/amt-13-951-2020.

[9] N.J. Popczun, L. Breuer, A. Wucher, N. Winograd, On the SIMS ionization probability of organic molecules, J. Am. Soc. Mass Spectrom. 28 (2017) 1182–1191. https://doi.org/10.1007/s13361-017-1624-0.

[10] A. Wucher, Molecular ionization probability in cluster-SIMS, J. Vac. Sci. Technol. B. 36 (2018) 03F123. https://doi.org/10.1116/1.5018305.

[11] C. Casiraghi, F. Piazza, A.C. Ferrari, D. Grambole, J. Robertson, Bonding in hydrogenated diamond-like carbon by Raman spectroscopy, Diam. Relat. Mater. 14 (2005) 1098–1102. https://doi.org/10.1016/j.diamond.2004.10.030.

[12] J.G. Buijnsters, R. Gago, I. Jiménez, M. Camero, F. Agulló-Rueda, C. Gómez-Aleixandre, Hydrogen quantification in hydrogenated amorphous carbon films by infrared, Raman, and x-ray absorption near edge spectroscopies, J. Appl. Phys. 105 (2009) 093510. https://doi.org/10.1063/1.3103326.

[13] P. Minutolo, M. Commodo, A. Santamaria, G. De Falco, A. D'Anna, Characterization of flame-generated 2-D carbon nano-disks, Carbon. 68 (2014) 138–148. https://doi.org/10.1016/j.carbon.2013.10.073.

[14] M. Commodo, G. De Falco, A. Bruno, C. Borriello, P. Minutolo, A. D'Anna, Physicochemical evolution of nascent soot particles in a laminar premixed flame: from nucleation to early growth, Combust. Flame. 162 (2015) 3854–3863. https://doi.org/10.1016/j.combustflame.2015.07.022.

[15] P. Parent, C. Laffon, I. Marhaba, D. Ferry, T.Z. Regier, I.-K. Ortega, B. Chazallon, Y. Carpentier, C. Focsa, Nanoscale characterization of aircraft soot: a high-resolution transmission electron microscopy, Raman spectroscopy, X-ray photoelectron and near-edge X-ray absorption spectroscopy study, Carbon. 101 (2016) 86–100. https://doi.org/10.1016/j.carbon.2016.01.040.

[16] K.C. Le, C. Lefumeux, P.-E. Bengtsson, T. Pino, Direct observation of aliphatic structures in soot particles produced in low-pressure premixed ethylene flames via online Raman spectroscopy, Proc. Combust. Inst. 37 (2019) 869–876. https://doi.org/10.1016/j.proci.2018.08.003.

[17] X. Mercier, O. Carrivain, C. Irimiea, A. Faccinetto, E. Therssen, Dimers of polycyclic aromatic hydrocarbons: the missing pieces in the soot formation process, Phys. Chem. Chem. Phys. 21 (2019) 8282–8294. https://doi.org/10.1039/C9CP00394K.

[18] L. Sleno, The use of mass defect in modern mass spectrometry, J. Mass Spectrom. 47 (2012) 226–236. https://doi.org/10.1002/jms.2978.

[19] A. Sadezky, H. Muckenhuber, H. Grothe, R. Niessner, U. Pöschl, Raman microspectroscopy of soot and related carbonaceous materials: spectral analysis and structural information, Carbon. 43 (2005) 1731–1742. https://doi.org/10.1016/j.carbon.2005.02.018.

[20] M. Frenklach, A.M. Mebel, On the mechanism of soot nucleation, Phys. Chem. Chem. Phys. 22 (2020) 5314–5331. https://doi.org/10.1039/D0CP00116C.